Materials Science & Engineering A 578 (2013) 46–53

Contents lists available at SciVerse ScienceDirect

Materials Science & Engineering A

journal homepage: www.elsevier.com/locate/msea

Microstructural and mechanical characterizations of a novel HVOF-sprayed WC-Co coating deposited from electroless Ni–P coated WC-12Co powders

M. Jafari [a,b,*], M.H. Enayati [a,b], M. Salehi [a,b], S.M. Nahvi [b], C.G. Park [c]

[a] Department of Materials Engineering, Isfahan University of Technology, Isfahan 84156-83111, Iran
[b] Iranian Surface Research and Engineering Centre, Isfahan 84155-337, Iran
[c] Department of Materials Science and Engineering, Pohang University of Science and Technology (POSTECH), Pohang 790-784, Republic of Korea

ARTICLE INFO

Article history:
Received 25 February 2013
Received in revised form
16 April 2013
Accepted 18 April 2013
Available online 25 April 2013

Keywords:
WC-Co
Electroless plating
HVOF
Microstructure
Mechanical properties

ABSTRACT

In this research, a novel WC-Co coating was deposited from electroless Ni–P coated WC-12Co powders using high velocity oxygen fuel (HVOF) process. Toward this purpose, an electroless Ni–P plating process was used to develop a uniform Ni–P layer on the surface of WC-12Co powders. The obtained Ni–P coated powders were then used as HVOF feedstock material. Microstructural characteristics of the Ni–P coated WC-12Co powders and the resultant coating, which is denoted as Ni–P modified coating, were investigated using X-ray diffractometry (XRD) and high resolution field emission scanning electron microscopy (HR FE SEM). The micro-hardness, elastic modulus and fracture toughness measurements were executed to evaluate the mechanical properties of the Ni–P modified coating. For comparison, the same experiments were performed on two conventional HVOF sprayed WC-12Co and WC-17Co coatings. The Ni–P modified WC-12Co coating showed a dense structure with extremely low porosity of ~0.3% which was much lower than that of WC-12Co and WC-17Co coatings. Besides, it was observed that the Ni–P modified coating has undergone negligible decarburization of 2.6% as compared to conventional WC-12Co and WC-17Co coatings with that of 16.3 and 17.6%. The Ni–P modified coating showed the maximum hardness of ~11.45 GPa, while lower hardness values of 10.98 and 10.59 GPa were measured for the WC-12Co and WC-17Co coatings. The fracture toughness of Ni–P modified WC-12Co coating was found to be 9.86 MPa $m^{1/2}$, indicating 71.2 and 61.1% increase in comparison with WC-12Co and WC-17Co coatings, respectively.

1. Introduction

The WC-Co based thermal spray coatings provide an excellent combination of high hardness and wear resistance, high elasticity, chemical inertness and low friction. These unique properties make WC-Co coatings ideal candidates to enhance wear resistance of engineering components such as cutting tools, extrusion dies, rollers, etc [1–6]. The WC-Co coatings deposited by high velocity oxygen fuel (HVOF) thermal spray technique possess very dense structure and desired physical properties which make them attractive for a wide range of applications [7]. The researches show that HVOF sprayed WC-Co coatings can be employed as effective alternatives to electroplated hard chromium coatings in the manufacturing and repair of a variety of industrial parts such as gas turbine shafts [8,9], aircraft landing gear [7] and certain jet engine components [10]. This is due to the fact that HVOF sprayed WC-Co coatings have been shown to be more wear resistant, cost-effective and environment-friendly in comparison with electroplated hard chromium coatings [8,9,11].

The HVOF process provides advantages in depositing WC-Co coatings over other thermal spray techniques such as air plasma spray (APS) and detonation spray coating (DSC) processes. These advantages include higher velocity and lower peak temperature of WC-Co powders during HVOF which lead to the formation of highly dense coatings with larger fraction of retained WC and excellent adherence to the substrate [4,5,12–16].

However, compared to sintered WC-Co fabricated under controlled conditions, HVOF-sprayed WC-Co coatings still suffer from decomposition and decarburization during spraying process, causing formation of non-WC phases such as W_2C, W, and amorphous or nanocrystalline Co-W-C phase [3,5,17,18]. Numerous studies have shown the detrimental effects of these phases on mechanical and wear properties of the coatings [1,5,19–24]. Many efforts, therefore, have been made to suppress the extent of decarburization; e.g., using a gas shroud to introduce an inert gas in HVOF spraying [22], optimization of HVOF parameters such as fuel/oxygen ratio [6,25] and in-flight particle velocity [26]. More

* Corresponding author at: Isfahan University of Technology, Department of Materials Engineering, Isfahan 84156-83111, Iran. Tel.: +98 334 2622574; fax: +98 311 3912752.
E-mail address: majid_jafari@ma.iut.ac.ir (M. Jafari).

0921-5093/$ - see front matter © 2013 Elsevier B.V. All rights reserved.
http://dx.doi.org/10.1016/j.msea.2013.04.064

recently, Yuan et al. [27] produced WC-Co based coatings containing solid lubricants of Cu and MoS_2 using APS technique. They showed that decarburization of WC during APS was decreased due to the protection of Cu layer around initial powders. Moreover, Mateen et al. [4] reported that using near-nanostructured WC-Co feedstock powder having duplex cobalt layer increases the retained WC phase of WC-Co coating after HVOF process.

In this research, electroless Ni–P plating process was initially applied to develop a thin protective layer around individual WC-12Co powder particles. Electroless plating is a well-established method to produce uniform coating materials over all surfaces, regardless of shape, size, and electrical conductivity [28–30]. Then, the obtained Ni–P coated WC-12Co powders were used as the HVOF feedstock material to deposit coating which is denoted as Ni–P modified WC-12Co coating. The microstructural and mechanical properties of Ni–P modified WC-12Co coating were investigated and compared with those of conventional WC-12Co and WC-17Co coatings.

2. Materials and methods

2.1. Materials

Three different powders were used as HVOF feedstock materials: two commercial WC-12Co and WC-17Co powders from Metallisation Ltd. (with characteristics presented in Table1) and Ni–P coated WC-12Co powder. In the case of Ni–P coated powder, an electroless nickel plating process was employed to develop a thin layer of Ni–P with thickness of ~0.5–1.5 μm around individual WC-12Co particles.

The atomic absorption spectroscopy (Young Lin AAS-8010) was performed to identify the chemical composition of the binder phase for WC-12Co, WC-17Co and Ni–P coated WC-12Co powders. The results are summarized in Table 2.

St37 steel disks with size of Ø30 × 5 mm were used as substrate. The disks were prepared for spraying by grit blasting followed by degreasing with acetone. The mean surface roughness (R_a) of substrates was measured at ~15 ± 2 μm.

2.2. HVOF spray process

The powders of WC-12Co, WC-17Co and Ni–P coated WC-12Co were deposited using MET JET III HVOF torch (Metallization Ltd. at PACO, Isfahan, Iran) to form coating layers. The HVOF process parameters are listed in Table 3. The substrates were air cooled from the backside during spraying process.

To evaluate the porosity of coatings, the SEM images from coatings cross-section were digitized and analyzed using Clemex microscopy image analysis software. The mean surface roughness (R_a) values of as-sprayed coatings were measured by Taylor-Hobson roughness tester.

2.3. Microstructural characterization

The XRD patterns of WC-12Co, WC-17Co and Ni–P coated WC-12Co powders and the corresponding coatings were recorded with step size of 0.05°/1 s using a Philips diffractometer (40 kV) with CuKα radiation (k=0.15406 nm). The patterns were then characterized by PANalytical X'Pert HighScore software. Microstructural characterizations of powders and coatings were executed using High Resolution FE SEM (JEOL JSM-7401 F). Carbon content of the initial powders and the coatings was measured by an elemental analysis tool (Elementar Vario EL III, Germany) in order to determine the amount of carbon loss during the HVOF process.

2.4. Mechanical properties of coatings

The micro-hardness of the coatings was measured using a Buehler micro-indentation at room temperature with 2 Kg of applied load and dwell time of 20 s. The mean value of 10 indents taken along the mid-plane of the coatings was quoted as the micro-hardness.

The elastic modulus of the coatings were evaluated via applying nano-indentations (FIB/Nanoindenter, Helios-Pegasus, FEI company, USA) on the cross-section of the coatings under load of 300 g. The elastic moduli were derived from the initial slope of force–displacement curve during unloading, following the procedure of Oliver and Pharr [31].

The indentation fracture toughness of coatings was measured by taking indents on the coatings cross-section at the load of 5 kg. Again, 10 indents were performed for each coating. The SEM images of the indentations were examined to obtain the precise lengths of corner cracks. Then, quantitative analysis of the fracture toughness (K_{IC}) of the coatings was done assuming that the cracks generated from indentations are radial with the Palmqvist geometry, using the following equation [4,5]:

$$K_{IC} = 0.193(H_v d)\left(\frac{E}{Hv}\right)^{2/5}(a)^{-1/2} \quad (1)$$

where Hv and E are Vickers hardness and elastic modulus of the

Table 2
Chemical composition (wt%) of the binder phase for feedstock powders. (The error is ± 1%).

Material	Co	Ni	P	Total binder
WC-12Co	12.1	–	–	12.1
WC–17Co	17.2	–	–	17.2
Ni–P coated WC-12Co	11.7	5.5	0.4	17.6

Table 3
HVOF spray parameters.

Deposition parameter	Value
Spraying distance (mm)	350
Oxygen (cm^3/s)	13.8
Methane (cm^3/s)	4.3
Carrier gas (Nitrogen) (cm^3/s)	66.7
Oxygen/Fuel ratio	3.19
Powder feed rate (g/s)	0.67
Spray angle (deg.)	90

Table 1
Characteristics of as-received WC-12Co and WC-17Co powders.

Characteristic	Powder	
	WC-12Co	WC–17Co
Element (wt%)	W: balance, Co:12.1, C:5.28, others:0.8	W: balance, Co:17.2, C:5.18, others:0.7
Particle size (μm)	15–45	15–45
Carbide size (μm)	1–6	1–5

coatings, respectively; *a* the crack length from indenter corner, and *d* the half-diagonal of the Vickers indentation.

3. Results and discussion

3.1. Characterization of electroless Ni–P coated WC-12Co powders

The surface morphology and cross-section of initial WC-12Co and electroless Ni–P coated WC-12Co powders are shown in Fig. 1. As shown in Fig. 1(a,b), the as-received WC-12Co powders have spherical morphology and are highly porous. Fig. 1c shows that the Ni–P coated WC-12Co powders have retained their spherical morphology after electroless plating. The cross-section of the Ni–P coated WC-12Co powders (Fig. 1d) reveals that a dense and uniform Ni–P layer is formed in the vicinity of WC-12Co particles. The thickness of the Ni–P coating was measured using Clemex image analysis software and found to be in the range of ~0.5–1.5 μm. During electroless Ni–P plating, two chemical reactions are operating: first, a chemical oxidation reaction that releases electrons in the solution and second, Ni ions reduction that consumes the electrons [32]. Nickel sulfate and sodium hypophosphite are widely used in electroless Ni–P plating as the preferred source of nickel cations and the reducing agent, respectively. The basic steps of plating process include diffusion and adsorption of the reactants (Ni^{2+} and $H_2PO_2^-$) on the surface, chemical reaction on the surface and desorption of the products (HPO_3^-, H_2 and H^+) [32]. For effective adsorption of the reactant materials, a surface with a high catalytic activity is required. As for solid materials, the surface catalytic activity is associated with the number of surface defects per unit area (such as the surface of the adsorbent edges and steps) [29]. Therefore, surface pretreatment and activation is usually required prior to the electroless plating. However, the WC-12Co powder particles used in this study were not subjected to any pretreatment. Detailed examination of WC-12Co surface morphology (Fig. 1a high magnification) proves the existence of a large number of edges and steps which considerably increase the specific surface area leading to the high catalytic activities. These morphological features cause an effective adsorption, nucleation and growth of Ni–P phase on the WC-12Co powders surface. When the electroless plating continues, a Ni–P coating with strong bonding and negligible fragmented parts is formed around individual WC-12Co particles. The resultant Ni–P coated WC-12Co powder particles were then used as HVOF feedstock powders.

3.2. Characterization of HVOF-sprayed coatings

3.2.1. Microstructural characteristics

Fig. 2 shows the SEM images of HVOF sprayed WC-12Co, WC-17Co and Ni–P modified WC-12Co coatings cross-sections.

The porosity percentage, in terms of the area fraction of pores, thickness and surface roughness of the coatings are presented in Table 4.

It is evident that the conventional WC-12Co and WC-17Co coatings possess the porosity levels of 1.6 and 1.3%, respectively. However, the Ni–P modified coating shows a negligible porosity percentage of ~0.3% which is about five and four times lower than that of WC-12Co and WC-17Co coatings. This suggests that utilizing the Ni–P coated WC-12Co as feedstock powder has led to formation of denser coating with improved inter-splat cohesion. Moreover, the Ni–P modified coating provides the lower surface roughness (~5.1 μm) value and smaller standard deviation.

The XRD patterns of WC-12Co, WC-17Co and Ni–P coated WC-12Co powders and the corresponding coatings are presented in Fig. 3.

The WC-12Co and WC-17Co powders are composed of WC and Co phases. As for the Ni–P coated WC-12Co powder, beside the WC

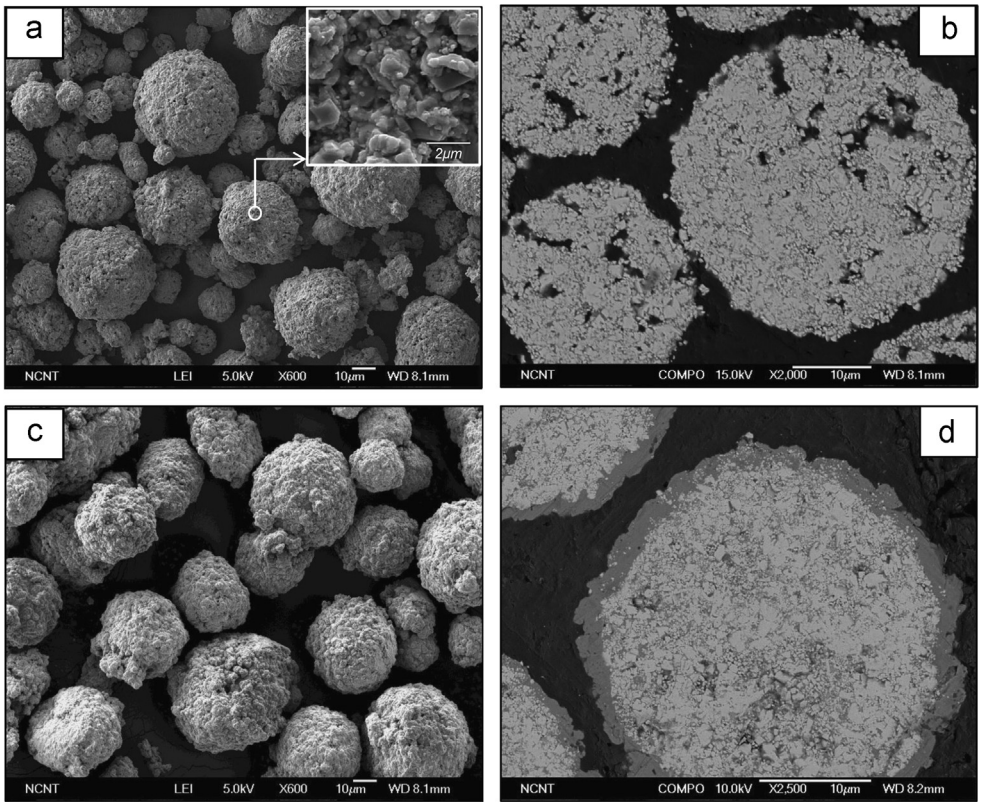

Fig. 1. SEM images of morphology and cross-section of initial WC-12Co (a,b) and electroless Ni–P coated WC-12Co (c,d) powders.

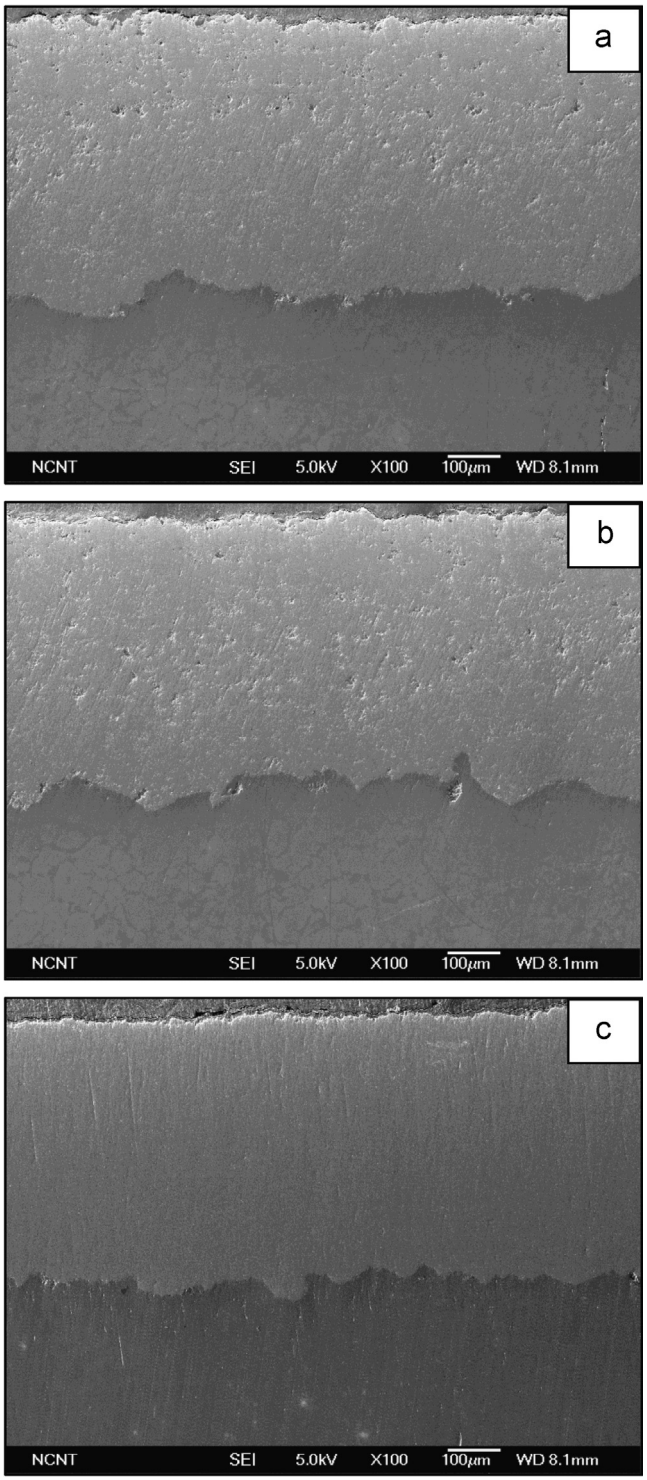

Fig. 2. SEM images showing cross-sections of as-sprayed (a) WC-12Co, (b) WC–17Co and (c) Ni–P modified WC-12Co coatings.

Table 4
Comparison between the characteristics of different coatings.

Coating	Porosity (%)	Thickness (μm)	Surface roughness R_a (μm)
WC-12Co	1.6 ± 0.5	417 ± 25	5.6 ± 0.6
WC–17Co	1.3 ± 0.6	432 ± 33	5.4 ± 0.5
Ni–P modified WC-12Co	0.3 ± 0.1	420 ± 15	5.1 ± 0.3

phase as the main constituent, two peaks corresponding to Ni and/or Co phases are present. The XRD pattern of WC-12Co coating shows the presence of W_2C and η (Co_6W_6C) phases, while no free cobalt peak was detected suggesting that cobalt has reacted with carbon and tungsten to form η (Co_6W_6C) phase. The W_2C peaks are also present on the XRD pattern of WC-17Co coating. Hence, it is obvious that the WC phase is significantly decomposed and decarburized during HVOF process of WC-12Co and WC-17Co coatings. Contrary to the WC-12Co and WC-17Co coatings, the XRD pattern of Ni–P modified coating (Fig. 3b (3)) reveals the presence of WC and Ni (Co) peaks along with a very small W_2C peak; furthermore, no η phase is observed on the XRD pattern. This structure verifies that the Ni–P modified coating has undergone negligible decarburization during HVOF process.

To evaluate the extent of decarburization of WC during HVOF process, a quantitative estimation of the amount of carbide phases in the initial powders and the resultant coatings was done using the XRD analysis [6]. Moreover, to measure the amount of carbon loss through HVOF process, carbon content of the initial powders and the coatings were compared. The results are summarized in Table 5.

According to the data given in Table 5, it is clear that the Ni–P modified coating contains the highest fraction of retained WC phase (97.9 wt%) after HVOF as compared to both conventional WC-12Co and WC-17Co coatings. The ratio of W_2C/WC peak intensities also proves the lowermost degree of decarburization in the case of Ni–P modified coating.

The percentage of decarburization is further estimated by comparing the carbon content in the initial powders and coatings [6]. The results, once again, ascertain insignificant decarburization of WC for Ni–P modified coating with carbon loss value of 2.6%, while the WC-12Co and WC-17Co coatings suffer from higher level of decarburization with carbon loss values of 16.3 and 17.6%, respectively. Therefore, one can conclude that the extensive decarburization of WC during HVOF can be prevented utilizing the Ni–P protective layer on WC-Co feedstock powders.

In order to realize the influence of using Ni–P coated powders on minimizing WC decarburization, the microstructural features of the WC-12Co and Ni–P modified WC-12Co coatings were examined in detail. Fig. 4 shows backscattered SEM image of the WC-12Co coating.

Two distinct regions are present in the microstructure of WC-12Co coating. The first region consists of a relatively dark matrix (representing low mean atomic number) in which the blocky carbide grains with sharp edges are distributed. This means that low level of WC dissolution into the matrix and consequently low level of decarburization is occurred so that the carbides tended to retain their initial faceted structure [1,18,33]. The second region, however, includes a brighter matrix (representing a higher mean atomic number) in which carbides show rounded morphology. Additionally, the presence of irregular bright fringes, identified as W_2C phase [18,33], is observed around some carbide particles; therefore, it is obvious that severe decarburization has occurred in the second region. According to the literature [1,5,18,33–36], the high temperature of HVOF flame causes the melting of cobalt binder phase. This is followed by the WC dissolution into the liquid binder enriching the adjacent cobalt matrix in tungsten and carbon elements. As a result of oxidizing atmosphere of HVOF flame, the carbon dissolved in the binder is oxidized to form CO/CO_2. Then, W_2C phase precipitates from the W-rich binder during solidification. Similar morphological features were observed for WC-17Co coating.

The backscattered SEM image of Ni–P modified WC-12Co coating is displayed in Fig. 5.

Contrary to the conventional coatings, the Ni–P modified coating exhibits more homogenous microstructure in which the

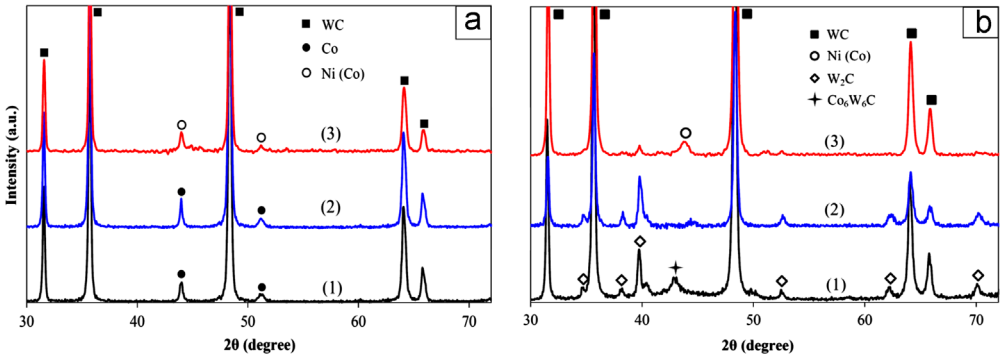

Fig. 3. XRD patterns of (a) feedstock powders and (b) as-sprayed coatings; (1) WC-12Co, (2) WC–17Co, (3) Ni–P modified WC-12Co.

Table 5
The amount of carbide phases and carbon element in the initial powders and resultant coatings derived from XRD data and elemental analysis.

Composition		Carbide phase (wt%)			Carbon element (wt%)	
		WC	W_2C	W_2C/WC	Carbon	Carbon loss
WC-12Co	Powder	100	–	–	5.28 ± 0.01	16.3
	Coating	90.6	9.4	0.1	4.42 ± 0.05	
WC–17Co	Powder	100	–	–	5.18 ± 0.01	17.6
	Coating	88.4	11.6	0.13	4.27 ± 0.03	
Ni–P modified WC-12Co	Powder	100	–	–	5.08 ± 0.01	2.6
	Coating	97.9	2.1	0.02	4.95 ± 0.03	

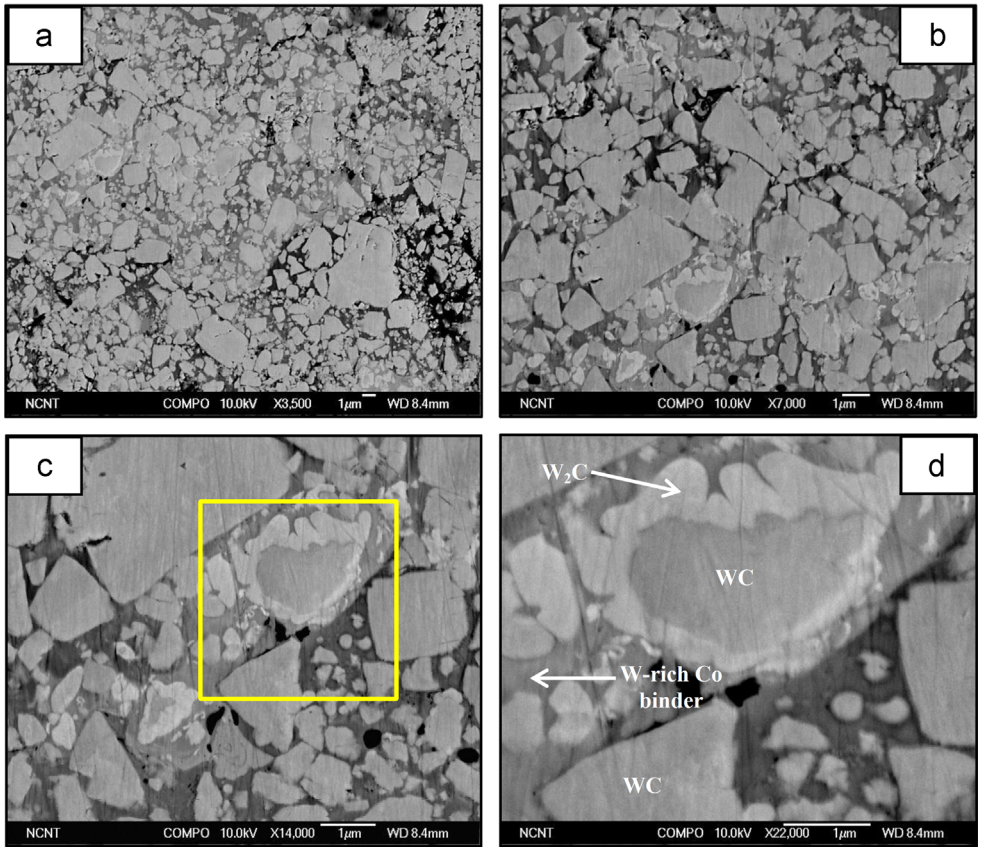

Fig. 4. Backscattered SEM images of WC-12Co coating microstructure at different.magnifications (a–d).

faceted WC grains are observed within the dark matrix. This feature can be approximately seen throughout the coating microstructure so that even very small carbides (see Fig. 5d), which are more susceptible to decarburization [5,14,19,37–39], present blocky morphology with sharp edges as in the initial powders. Therefore, in agreement with XRD analysis, the Ni–P modified

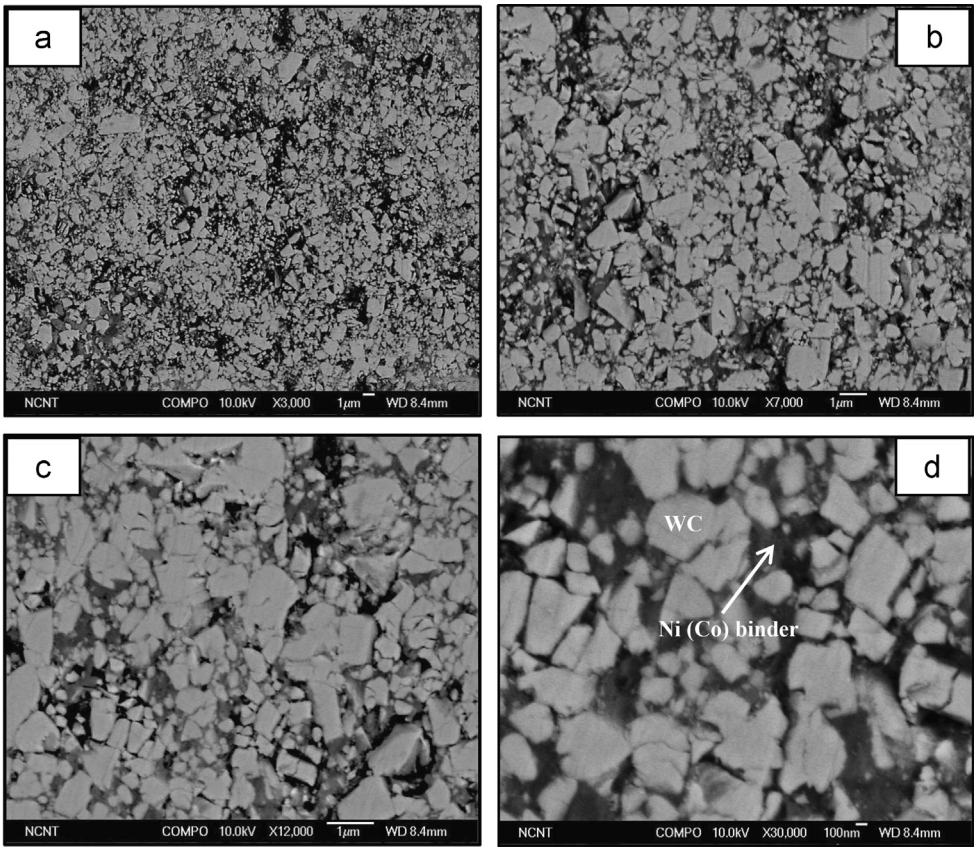

Fig. 5. Backscattered SEM image of Ni–P modified WC-12Co coating microstructure at different magnifications (a–d).

WC-12Co coating experienced no significant decarburization during HVOF. The mechanisms by which the Ni–P layer on WC-12Co powders reduces the extent of decarburization can be explained from two aspects. On one hand, as a result of high HVOF flame temperature, the Ni–P outer layer melts and absorbs latent heat of fusion decreasing the heating degree of inner WC-Co particles. This causes less WC dissolution into the matrix, less subsequent carbon oxidation, and accordingly the lower extent of decarburization. The lower the decarburization level, the less the CO/CO_2 formation occurs during HVOF [4,40], resulting in the deposition of highly dense Ni–P modified coating with minimum internal porosity (0.3%), as shown in Fig. 2. On the other hand, the Ni–P layer can effectively reduce the WC exposure to oxidizing flame. This prevents direct WC oxidation which is considered as another mechanism for W_2C formation during HVOF process, as proposed by Guilemany et al. [18].

3.3. Mechanical properties

The Vickers micro-hardness and elastic modulus of WC-12Co, WC-17Co and Ni–P modified WC-12Co coatings are presented in Fig. 6.

It is evident that the Ni–P modified coating shows the maximum hardness of ~11.45 GPa, while lower hardness values of 10.98 and 10.59 GPa were obtained for the WC-12Co and WC-17Co coatings, respectively (Fig. 6a). The hardness of the coating is affected by the microstructure, phase composition (WC, W_2C, and amorphous phase), porosity, etc [5]. The reason why the Ni–P modified coating presents the highest hardness can be attributed to its low porosity and high inter-splat cohesion [35]. Moreover, the least scattering of hardness data was found for Ni–P modified coating pointing to the high microstructure uniformity [5].

The elastic modulus of the coatings was obtained using the nano-indentation tests on the polished cross-section of the coatings. The results, provided in Fig. 6b, shows approximately similar elastic modulus of ~300 GPa for WC-12Co and Ni–P modified WC-12Co coatings, while slightly lower value of ~295 GPa was found for WC-17Co coating. The measured elastic moduli for the coatings are in agreement with those reported by Chivavibul et al. [5] and Lima et al. [41].

Fig. 7 (a–c) illustrates the typical SEM images of Vickers indentations formed on the cross-section of the coatings.

In all cases, indentation cracks have propagated only in the direction parallel to the coating/substrate interface, indicating the substantial anisotropic behavior for toughness of the coatings; i.e., low and high amounts of fracture toughness in the directions parallel and perpendicular to the coating/substrate interface, respectively. This anisotropy is due to the lamellar structure of coatings in which the lamellae interface is disposed to decohesion; hence, the cracks initiated under indentation test develop in the direction parallel to lamellae. Fig. 7d compares the fracture toughness of WC-12Co, WC-17Co and Ni–P modified coatings. The Ni–P modified WC-12Co coatings shows a maximum fracture toughness of 9.86 MPa $m^{1/2}$ as compared to WC-12Co and WC-17Co coatings with that of 5.76 and 6.12 MPa $m^{1/2}$, respectively. This represents 71.2 and 61.1% increase in the fracture toughness for the Ni–P modified coating compared with WC-12Co and WC-17Co coatings. It is well-documented that the presence of brittle W_2C and η phases reduces the fracture toughness of cemented carbide coatings [4–6,19,42–44]. Therefore, the Ni–P modified coating, which contains negligible amount of W_2C and η (Co_6W_6C) phases, presents higher fracture toughness. Concurrently, lower degree of decarburization for Ni–P modified coating decreases the extent of W-rich binder regions (see Fig. 5), which are considered as preferential paths for crack propagation [5,19]. In addition, the

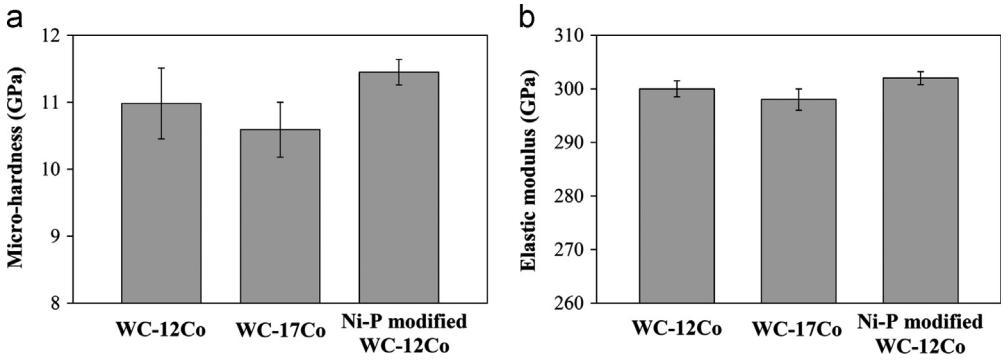

Fig. 6. Plots of (a) micro-hardness and (b) elastic modulus for WC-12Co, WC–17Co and Ni–P modified WC-12Co coating.

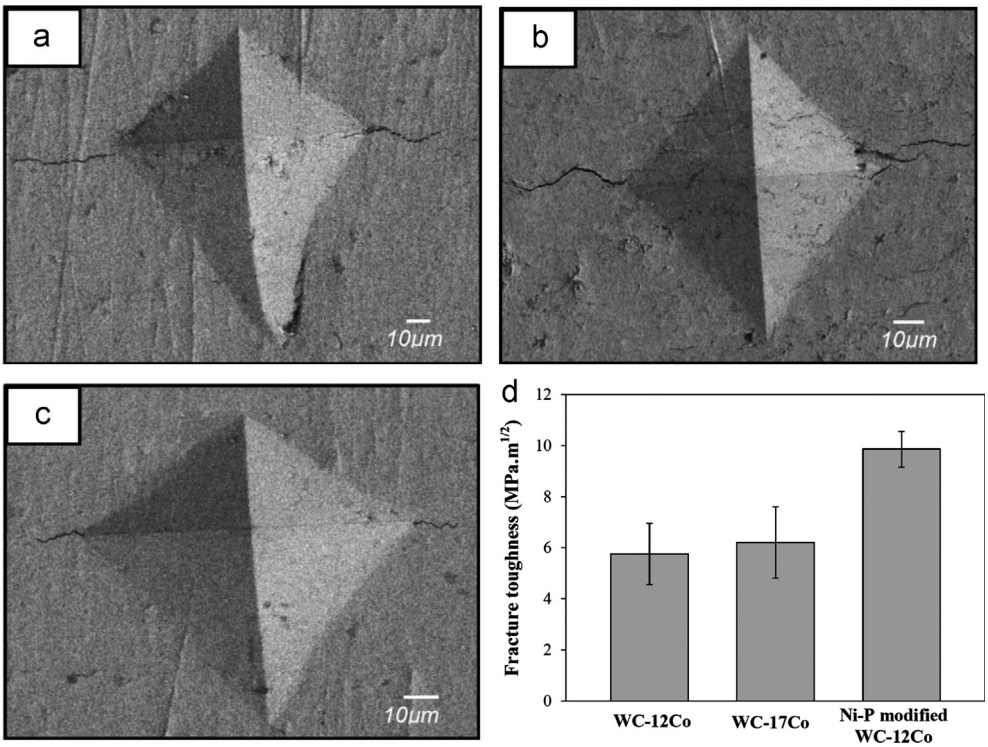

Fig. 7. Typical SEM images indicating Vickers indentations performed at a load of 5 kg on the cross-section of (a) WC-12Co, (b) WC–17Co and (c) Ni–P modified WC-12Co coatings. (d) Plot of average facture toughness of the coatings measured after taking 10 indents.

dense structure and improved splat cohesion observed for Ni–P modified coating can suppress the crack propagation through the coating lamellae.

4. Conclusions

In this study, the microstructural and mechanical properties of a novel Ni–P modified WC-12Co coating deposited by HVOF method were evaluated and compared with two conventional WC-12Co and WC-17Co coatings. The following conclusions can be drawn:

- The electroless Ni–P plating resulted in the formation of a dense and uniform Ni–P coating layer with thickness of ~0.5–1.5 μm on the surface of WC-12Co powders. The Ni–P coated WC-12Co particles were then used as feedstock powders of HVOF process.
- The Ni–P modified coating showed a negligible porosity percentage of ~0.3% which was about five and four times lower than that of WC-12Co and WC-17Co coatings, respectively. Besides, the Ni–P modified coating indicated the lower surface roughness value with a lower standard deviation among the coatings.
- Regarding the microstructural characterizations, it was observed that utilizing Ni–P coated WC-12Co feedstock powder significantly reduces the extent of decarburization; i.e., the Ni–P modified coating has undergone negligible decarburization of 2.6%, while the WC-12Co and WC-17Co coatings suffer from more decarburization with carbon loss values of 16.3 and 17.6%.
- The Ni–P modified coating showed the maximum hardness of ~11.45 GPa, while lower hardness values of 10.98 and 10.59 GPa were obtained for the WC-12Co and WC-17Co coatings, respectively. The elastic modulus measurements indicated approximately similar value of ~300 GPa for WC-12Co and Ni–P modified WC-12Co coatings, and marginally lower value of ~295 GPa for WC-17Co coating.

– The maximum fracture toughness of 9.86 MPa.m$^{1/2}$ was found for Ni–P modified WC-12Co coating, representing 71.2 and 61.1% increase as compared with WC-12Co and WC-17Co coatings, respectively.

References

[1] N.S. Lim, S. Das, S.Y. Park, M.C. Kim, C.G. Park, Surf. Coat. Technol. 205 (2010) 430–435.
[2] G.C. Saha, T.I. Khan, Metal, Mater. Trans. A 41A (2010) 3000–3009.
[3] P. Chivavibul, M. Watanabe, S. Kuroda, J. Kawakita, M. Komatsu, K. Sato, J. Kitamura, J. Therm.Spray Technol. 20 (5) (2011) 1098–1109.
[4] A. Mateen, G.C. Saha, T.I. Khan, F.A. Khalid, Surf. Coat. Technol. 206 (2011) 1077–1084.
[5] P. Chivavibul, M. Watanabe, S. Kuroda, K. Shinoda, Surf. Coat. Technol. 202 (2007) 509–521.
[6] P. Suresh Babu, B. Basu, G. Sundararajan, Acta Mater. 56 (2008) 5012–5026.
[7] A. Ibrahim, C.C. Berndt, Mater. Sci. Eng. A 456 (2007) 114–119.
[8] T. Sahraoui, N.E. Fenineche, G. Montavon, C. Coddet, J. Mater, Process Technol. 152 (2004) 43–55.
[9] T. Sahraoui, N.E. Fenineche, G. Montavon, C. Coddet, Mater. Design 24 (2003) 309–313.
[10] Z. Mutasim, V. Bankar, C. Rimlinger, in: C.C. Berndt (Ed.), HVOF Thermal Sprayed Coatings as Alternates to WC–12%Co Coatings and Chromium Plating, ASM International, Materials Park, OH, USA, 1997, pp. 901–908.
[11] T. Sahraoui, S. Guessasma, N.E. Fenineche, G. Montavon, C. Coddet, Mater. Lett. 58 (2004) 654–660.
[12] M. Li, P.D. Christofides, Chem. Eng. Sci. 61 (2006) 6540–6552.
[13] B.R. Marple, R.S. Lima, J. Therm. Spray Technol. 14 (2005) 67–76.
[14] Z.G. Ban, L.L. Shaw, J. Therm. Spray Technol. 12 (1) (2003) 112–119.
[15] H.L. De Villiers Lovelock, J. Therm. Spray Technol. 7 (3) (1998) 357–373.
[16] J.R. Fincke, W.D. Swank, D.C. Haggard, in: C.C. Berndt, S. Sampath (Eds.), Comparison of the Characteristics of HVOF and Plasma Thermal Spray in Thermal Spray Industrial Applications, ASM International, Materials Park, OH, 1994, pp. 325–330.
[17] V.V. Sobolev, J.M. Guilemany, J. Nutting, High Velocity Oxy-fuel Spraying: Theory, Structure–Property Relationships and Applications, Maney Publishing, UK, 2004.
[18] J.M. Guilemany, J.M. de Paco, J. Nutting, J.R. Miguel, Metal. Mater. Trans. A 30A (1999) 1913–1921.
[19] D.A. Stewart, P.H. Shipway, D.G. McCartney, Wear 789 (1999) 225–229.
[20] S. Usmani, S. Sampath, D.L. Houck, D. Lee, Tribol. T. 40 (3) (1997) 470–478.
[21] C. Verdon, A. Karimi, J.L. Martin, Mater. Sci. Eng. A 246 (1–2) (1998) 11–24.
[22] Y. Ishikawa, J. Kawakita, S. Sawa, T. Itsukaichi, Y. Sakamoto, M. Takaya, S. Kuroda, J. Therm. Spray Technol. 14 (3) (2005) 384–390.
[23] M. Watanabe, A. Owada, S. Kuroda, Y. Gotoh, Surf. Coat. Technol. 201 (3–4) (2006) 619–627.
[24] Y. Ishikawa, S. Kuroda, J. Kawakita, Y. Sakamoto, M. Takaya, Surf. Coat. Technol. 201 (8) (2007) 4718–4727.
[25] P. Suresh Babu, B. Basu, G. Sundararajan, Wear 268 (2010) 1387–1399.
[26] G.C. Saha, T.I. Khan, L.B. Glenesk, J. Nanosci. Nanotechnol. 9 (2009) 4316–4323.
[27] J. Yuan, Y. Zhu, X. Zheng, H. Ji, T. Yang, J. Alloys Compd. 509 (2011) 2576–2581.
[28] L. Luo, Y. Wu, J. Li, Y. Zheng, Surf. Coat. Technol. 206 (2011) 1091–1095.
[29] W.H. Lin, H.F. Chang, Surf. Coat. Technol. 107 (1998) 48–54.
[30] S.S. Zhang, K.J. Han, L. Cheng, Surf. Coat. Technol. 202 (2008) 2807–2812.
[31] W.C. Oliver, G.M. Pharr, J. Mater. Res. 7 (1992) 1564–1583.
[32] G.O. Mallory, J.B. Hajdu (Eds.), Electroless Plating Fundamental and Applications, American Electroplaters and Surface Finishers Society, 1990.
[33] D.A. Stewart, P.H. Shipway, D.G. McCartney, Surf. Coat. Technol. 105 (1998) 13–24.
[34] J. He, J.M. Schoenung, Mater. Sci. Eng. A 336 (2002) 274–319.
[35] C.J. Li, A. Ohmori, Y. Harada, J. Mater. Sci. 31 (1996) 785–794.
[36] H. Chen, G. Gou, M. Tu, Y. Liu, J. Mater. Eng. Perform. 19 (1) (2010) 1–6.
[37] J. He, M. Ice, S. Dallek, E.J. Lavernia, Metal. Mater. Trans. A 31A (2000) 541–553.
[38] B.H. Kear, G. Skandan, R.K. Sadangi, Scripta Mater. 44 (2001) 1703–1707.
[39] D.A. Stewart, P.H. Shipway, D.G. McCartney, Acta Mater. 48 (2000) 1593–1604.
[40] J.M. Guilemany, S. Dosta, J. Nin, R. Miguel, J. Therm. Spray Technol. 14 (2005) 405–413.
[41] R.S. Lima, S.E. Kruger, G. Lamouche, B.R. Marple, J. Therm. Spray Technol. 14 (2005) 52–60.
[42] Y. Qiao, Y. Liu, T.E. Fischer, J. Therm. Spray Technol. 10 (2001) 118–125.
[43] J.M. Guilemany, S. Dosta, J.R. Miguel, Surf. Coat. Technol. 201 (2006) 1180–1190.
[44] H. Liao, B. Normand, C. Coddet, Surf. Coat. Technol. 124 (2000) 235–242.